ELSEVIER

Journal of Wind Engineering
and Industrial Aerodynamics 56 (1995) 185–212

JOURNAL OF wind engineering AND industrial aerodynamics

Long time-averaged solutions of turbulent flow past a circular cylinder

Ismail Celik[a,*], Franklin D. Shaffer[b]

[a] *Mechanical and Aerospace Engineering Department, West Virginia University, Morgantown, WV 26506, USA*

[b] *United States Department of Energy, Pittsburgh Energy Technology Center, Pittsburgh, PA 15236, USA*

Received 8 November 1993; accepted in revised form 22 July 1994

Abstract

A critical analysis of numerical predictions of the long time averaged flow past a circular cylinder is presented. The flow regimes considered cover a wide range of Reynolds numbers with an emphasis on the transitional range, i.e. (10^4 to 10^7). In this study calculations are made using the standard k–ε model with an empirically imposed transition criteria. Our own simulations as well as those published by others with various turbulence models including those with vortex shedding are compared with experimental data. Significant differences were found among different predictions for the same flow conditions with essentially the same turbulence models. Reasons for these differences are elucidated. The transitional nature of the flow regime, and the grid size and its distribution, particularly inside the boundary layer, play a major role in obtaining vastly different predictions. The present calculations with the conventional k–ε turbulence model and an empirically imposed transition compare favorably with those obtained from "more sophisticated" models such as large-eddy simulations.

1. Introduction

In spite of the simple geometry, numerical simulation of turbulent flow past a circular cylinder still remains a challenging problem for computational fluid dynamicists. The simulations of Majumdar and Rodi [1] the review by Celik [2] and Celik and Shaffer [3] showed that there are significant differences between calculated and measured mean flow parameters. Furthermore, simulations using the standard k–ε model, similar numerical procedures, and similar numbers of grid cells often produce predictions with striking differences. The discrepancies between experiments

* Corresponding author.

SSDI 0167-6105(94)00091-3

and numerical simulations do not uniformly reduce as one increases the order of closure models for turbulence. In this paper, we present an analysis of these simulations and discuss possible reasons for differences among them. For completeness, we first present a brief description of the general flow characteristics followed by a review of previous calculations.

1.1. General features of the flow

In the Reynolds number, Re, range considered (10^4 to 10^7) the flow around a nominally "smooth" circular cylinder undergoes transitional changes. Four different flow regimes are identified each marked by a different behavior of the boundary layer. In the literature, various terminologies are used for these regimes by different authors (see, e.g., Ref. [4]). Here we adapt the terminology suggested by Achenbach [5] according to which the four flow regimes are (see Fig. 1): (i) subcritical, (ii) critical, (iii) supercritical and (iv) transcritical. The Reynolds numbers marking the beginning and the end of each regime can vary significantly for different experimental setups depending on the actual values of surface roughness, free-stream turbulence intensity and length scale, wind-tunnel blockage, length to diameter ratio, and model-end conditions. However, for "smooth" cylinders the following approximate ranges can be used as a basis for discussion: (i) subcritical flow, $2.0 \times 10^2 < \mathrm{Re} < 1.5 \times 10^5$; (ii) critical flow, $1.5 \times 10^5 < \mathrm{Re} < 4 \times 10^5$; and (iii) super critical flow, $4 \times 10^5 < \mathrm{Re} < 1. \times 10^7$; (iv) transcritical flow, $\mathrm{Re} > 1 \times 10^7$.

In the subcritical flow regime the boundary layer remains completely laminar, the drag coefficient, $C_D \simeq 1.0$–1.2, remains fairly constant, the Strouhal number, $S \simeq 0.2$, and the location of separation, ϕ_s, is approximately 75° to 85°. The transition from laminar to turbulent flow in the shear-layers takes place in the formation region of the wake [6] and it moves gradually upstream as Re increases. In the critical range, C_D

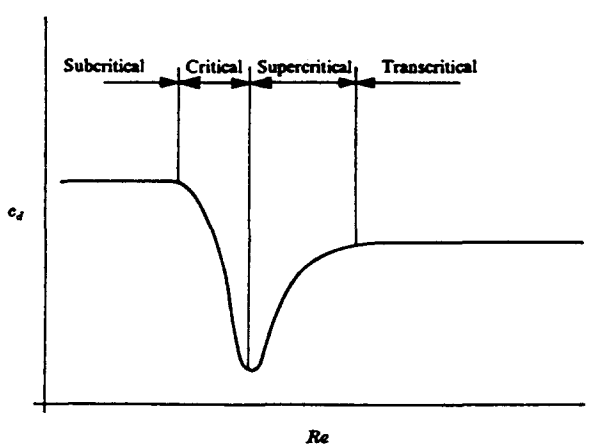

Fig. 1. Illustration of flow regimes for the flow past circular cylinders (after Ref. [5]).

decreases suddenly from 1.2 to about 0.25, S increases from 0.2 to about 0.5, the location of separation moves downstream to about $\phi_s = 120°–140°$. First a laminar separation occurs followed by turbulent reattachment and eventual turbulent separation thus forming the so-called "laminar separation turbulent reattachment-bubble". This regime is characterized by irregular vortex shedding, asymmetric formation of the bubble (i.e. on one or both sides of the cylinder), and lack of two-dimensionality (for a detail review and discussion of this regime see Refs. [4,7]). In the supercritical flow regime, C_D increases, S decreases to about 0.25, a fairly sharp transition occurs from laminar to turbulent flow prior to separation, and the separation point moves upstream to about $\phi = 105°–115°$. Finally, in the transcritical flow regime C_D reaches a new plateau, the transition point moves sufficiently close to the upstream stagnation point so that the location of separation is not influenced much by further increase in Re, hence the flow becomes independent of the Reynolds number.

1.2. Review of previous computations

Navier–Stokes solutions of the flow past circular cylinders have been the subject of numerous previous investigations. Most of these were reviewed by Majumdar and Rodi [1], Ishii et al. [8], and a broader review was presented by Celik [2]. For a long time Navier–Stokes solutions of the flow in question were limited to relatively low Reynolds numbers, $\mathrm{Re} < 10^4$. Recently, there has been a number of reports on the same subject at high Reynolds numbers. A detailed review of all the previous computational work is a formidable task and it is beyond the scope of this paper. Here we shall restrict our review to only those concerning the high Reynolds number range, $\mathrm{Re} > 10^4$. A summary of papers reviewed is presented in Table 1.

Sugavanam [9], and Sugawanam and Wu [10] reported solutions of the Navier–Stokes equations for a turbulent flow around a circular cylinder at $\mathrm{Re} = 3.6 \times 10^6$. They used a hybrid integro-differential approach, HIDA, and employed the standard k–ε (SKEM) model for most of the flow field while using a mixing length model near the cylinder surface (up to 0.12 radii from the cylinder surface). At a first glance their results seem to be in good agreement with measurements of Achenbach [11], but as it is shown later in this paper a close look into the results reveals that they did not account for the large blockage effects (i.e. effects of the presence of tunnel walls), and their grid resolution was rather coarse.

Majumdar and Rodi [1] calculated the mean flow past circular cylinders using a finite volume method in body fitted curvilinear coordinates as well as polar cylindrical coordinates. They used SKEM with an artificial transition imposed immediately after the separation point. The predicted pressure distribution, the location of separation, and the wall shear stress were not found satisfactory in comparison with measurements. These authors concluded that separated turbulent flow past circular cylinders cannot be predicted realistically with a steady-flow model ignoring the periodic vortex-shedding motion. The results of Majumdar and Rodi shall be discussed in detail in subsequent sections.

Ishii et al. [8] performed calculations in the range $1.0 \times 10^5 \leqslant \mathrm{Re} \leqslant 7.83 \times 10^6$. They used the Beam–Warming–Steger method with improved accuracy to solve the

Table 1
Summary of previous computations for $Re \geq 1.0 \times 10^4$ Navier–Stokes solutions

Ref.	Re	Turbulence model	Numerical method	Comments
[10]	3.6×10^6	SKEM and Mix. L.	HIDA	
[1]	1.0×10^5, 1.4×10^5, 3.6×10^6	SKEM	FVOL	polar grid, steady
[8]	1.0×10^5–7.83×10^6	(none)	FDIF	BFC grid, 2D unsteady
[13]	1.4×10^5, 8.4×10^6	2D-PLES	FVOL	non-orthogonal non-structured grid, unsteady
[12]	1.0×10^4 1.0×10^6	(none)	FDIF	2D and 3D unsteady 3rd order upwind
[18]	1.4×10^4	2ZKE 2ZLRR	FVOL	QUICK scheme, 2D unsteady
[19]	1.0×10^4	LED 2D-PLES	FELM	upwind scheme, unsteady

Notation: SKEM, standard k–ε model; LES, large-eddy simulation; PLES, pseudo-large-eddy simulation; 2ZKE, two-zone k–ε model; 2ZLRR, two-zone Launder–Reece–Rodi (Reynolds stress transport) model; HIDA, hybrid integro-differential approach; FVOL, finite volume; FDIF, finite difference; FELM, finite element; BFC, body fitted coordinates.

two-dimensional Navier–Stokes equations directly without any turbulence model. They did not apply any explicit filtering to set the scale of the dissipative mechanism. Their smallest mesh size in the direction normal to the cylinder surface was 1×10^{-5} cylinder diameters with a grid distribution of 481×120 in the whole plane. The predicted drag coefficient was in good agreement with experiments in this Re range; the predictions being generally lower than the measurements. The results showed a transition from subcritical to supercritical regime, the recovery from critical regime was significantly slower compared to the experiments. These predictions were found to be grid dependent by Tamura et al. [12].

Song and Yuan [13] presented calculations with a two-dimensional, pseudo-large eddy simulation (2D-PLES) model. They used an explicit finite volume method with MacCormack's predictor–corrector scheme. The subgrid scale constant was selected as 0.15 instead of 0.21 which was originally suggested for the Simagorinsky model. In the boundary layer, they introduced some ad hoc modifications. In this sense their calculations seem to be fine tuned especially for this particular flow. They simulated Cantwell and Coles' [14] experiments ($Re = 1.4 \times 10^5$) and obtained good agreement of velocity distribution in the wake, however the pressure distribution did not agree well with Cantwell and Coles' measurements (see also discussions in subsequent sections). Song and Yuan also calculated a case in supercritical flow regime at

$Re = 8.4 \times 10^6$. The comparison of the predicted pressure distribution with Roshko's [15] measurements showed also good agreement between the two. It should be noted that these two-dimensional calculations are not really large-eddy simulations, because large-eddy simulations must be, by definition, three-dimensional and unsteady [16]. Hence the terminology PLES is used in the present discussion.

Tamura et al. [12] presented a very interesting paper where they simulated the unsteady flow past cylindrical structures with a relatively accurate third order upwind finite difference scheme. They employed no turbulence model. The grid they used is slightly skewed, nearly orthogonal polar cylindrical grid. Their calculations demonstrated that the numerical solutions were highly sensitive to grid fineness. In particular they showed that at $Re = 10^5$ coarser grids lead to solutions with critical and supercritical characteristics and very fine grid solutions showed subcritical characteristics. The most sensitive range was in the critical flow regime, i.e. $1.0 \times 10^4 < Re < 1.0 \times 10^6$. This is not surprising given the fact that the flow is very sensitive to any kind of disturbance in this regime (see, e.g., Refs. [4,7]). Tamura et al. showed that the three-dimensional calculations, in this regime, were in better agreement with experiments compared to the two-dimensional calculations. This should be expected since the actual flow in the critical regime is highly three-dimensional [4,7,17]. They were able to predict the transition from subcritical flow to supercritical flow without employing any turbulence model or imposing any filtering. This might be explained on the basis of large-eddy simulations [16] with a self-induced filtering mechanism by the numerical scheme itself.

A detailed numerical analysis of the unsteady flow past a circular cylinder at $Re = 1.4 \times 10^5$ was presented by Franke [18]. He used the well-known QUICK scheme in spatial coordinates and a first order implicit scheme in the temporal domain. Two different turbulence models were implemented, namely, a two-zone k–ε, 2Z-KE, model, and a two-zone Reynolds stress (Launder, Reece and Rodi model), 2Z-LRR, model. The two-zone refers to using the one equation model in the vicinity of the wall where the k-equation is solved but ε is determined from an empirical algebraic equation. Modifications were also made by Franke to account for the low Reynolds number nature of the flow in the boundary layer. He presented time averaged pressure distributions for Cantwell and Coles' [14] experiments. The 2Z-KE model resulted in significantly higher base pressure, which is believed to be the inherent deficiency of steady calculations [1]. The 2Z-LRR model gave somewhat better agreement with the measured distribution except in the vicinity of the rear stagnation point. Franke's results should show the influence of unsteady calculations, i.e. the influence of vortex shedding, as compared to steady mean flow calculations. But the unsteady calculations with the KE model still resulted in a high base-pressure coefficient even though the vortex shedding is taken into account. A detailed discussion of his results follows later in the text.

Kato and Ikegawa [19] presented large-eddy simulations (LES), for the flow past circular cylinders. They used a streamline upwind finite element method with the classical Smagorinsky subgrid scale model to solve the unsteady three-dimensional equations of motion. The blockage effects were eliminated via appropriate boundary conditions at a distance of 10 diameters away from the cylinder surface. The grid used

was $80 \times 50 \times 10$, in circumferential, normal and axial directions, respectively. They imposed an empirical transition to laminar flow in the sublayer by arbitrarily damping the turbulent eddy viscosity within one fifth of a diameter from the cylinder surface. They presented results for a case with $\mathrm{Re} = 1.0 \times 10^4$ from both 3D-LE simulations and 2D-PLE simulations which seem to indicate that the former (3D-LES) gives better agreement with the measurements of Cantwell and Coles [14] at $\mathrm{Re} = 1.4 \times 10^5$ compared to the latter (2D-PLES). However, as discussed later, it is very likely that their results are grid dependent.

1.3. Present contribution

As it is seen from the above review there seems to be many unresolved issues concerning the Navier–Stokes solutions of the turbulent flow past circular cylinders. Some of the major issues which should be addressed are the grid dependency of the solutions, the blockage effects, transition to turbulent flow, resolution of the boundary layer, two-dimensional versus three-dimensional, steady versus unsteady calculations, and the assessment of the relative performance of various turbulence models. There is also the question and a mixed opinion as to how good the results calculated by using the classical turbulence closure models, e.g. the k–ε model are. In this paper we attempt to make an assessment of these issues with the help of our own calculations using a finite volume method with the standard k–ε model. We present two-dimensional long time-averaged solutions and compare them with solutions with more sophisticated simulations as well as large-eddy simulations with the objective of assessing the performance of relatively simple and inexpensive calculations compared to others. This issue is important in large scale industrial applications, such as gas-solid two phase flow past heat exchanger tubes in boilers, and ocean currents past an array of platform supports. For such problems the time and cost involved in utilizing, for example, large-eddy simulations are still not at an affordable level.

2. Computational details

Simulations were performed using a commercial code, PHOENICS [20]. It is based on the well-known SIMPLE algorithm [21] and uses a control volume approach with a hybrid of upwind and central differencing schemes. The two-dimensional Navier–Stokes or Reynolds equations written in terms of the primitive variables (i.e., the two velocity components and the pressure) for an incompressible fluid are solved. Several options are available for the turbulence models, but for this work only the standard k–ε model [22] was utilized. The equations for this model are given in Appendix A for reference. The turbulence model constants were $k = 0.435$, $E_{\mathrm{wall}} = 9$, $C_{\mathrm{d}} = 0.1643$, $C'_{\mu} = 0.5478$ ($C_{\mu} = C_{\mathrm{d}}$, $C'_{\mu} = 0.09$), $C_{1\varepsilon} = 1.44$, $C_{2\varepsilon} = 1.92$, $\sigma_k = 1.0$ and $\sigma_{\varepsilon} = 1.314$. The notation for these constants are the standard notation (see, e.g. Ref. [22], see also Appendix A) the turbulence length scale is calculated from

$$l_t = C_{\mathrm{d}} k^{1.5}/\varepsilon \tag{1}$$

and the turbulent eddy viscosity is calculated from

$$v_t = C'_\mu l_t k^{1/2}, \tag{2}$$

where k is the turbulent kinetic energy and ε is the dissipation rate of k.

2.1. Transition to turbulence

For the present calculations transition to turbulence was imposed by resetting l_t such that a sufficiently small value of v_t (e.g. $v_t \ll v$, v being the kinematic viscosity) resulted from Eq. (2) in the laminar flow regions. Transitional values for l_t (hence for v_t) were calculated by interpolation using a power law between the fully laminar and fully turbulent regions; downstream of the transition region it was calculated from Eq. (1). A similar transitional model was also applied by Majumdar and Rodi [1]. The location of the transition was determined using an empirical equation suggested by Celik et al. [23] as a guide; which is

$$x_{tr}/D = 0.15(\mathrm{Re}_{bc}/\mathrm{Re})^{1/2}, \tag{3}$$

where $\mathrm{Re}_{bc} \simeq 1.5 \times 10^5$ is the Reynolds number marking the beginning of the critical flow regime. This equation gives the distance to transition location, x_{tr}, as a function of the cylinder Reynolds number up to the beginning of the critical flow regime, e.g. $\mathrm{Re} = 1.5 \times 10^5$. However, sensitivity analysis is performed by changing the transition location as one of the unknown parameters. For more details see Ref. [23] or Ref. [3].

2.2. Boundary conditions

At the inlet uniform profiles were specified for axial velocity, U, and the y-component of the velocity, V, was set to zero (see Fig. 2 for notation). For cylindrical-polar grids the fixed Cartesian inlet velocity in the x-direction was converted to variable components in the r- and ϕ-directions. In this case, the circular arc $r = 10d$, $0 \leqslant \phi < \pi/2$ formed the inlet boundary, and $r = 10d$, $\pi/2 \leqslant \phi \leqslant \pi$ formed the outlet boundary; ϕ is measured from the upstream stagnation point clockwise (see Fig. 2). The velocities thus prescribed varied only 0.25% from the attached potential flow solutions. The turbulent kinetic energy was calculated from the experimentally specified turbulence intensity and ε was calculated from

$$\varepsilon = k^{3/2}/ah, \tag{4}$$

where h is a characteristic length (i.e. the width of the wind tunnel) and a is a coefficient which was selected such that Eqs. (1) and (2) yielded sufficiently low turbulent eddy viscosity which typically was equal to the kinematic viscosity of the fluid. Uniform profiles were used for both k and ε at the inlet.

At the outlet convective outflow boundary conditions were imposed. This amounts to imposing zero first derivatives.

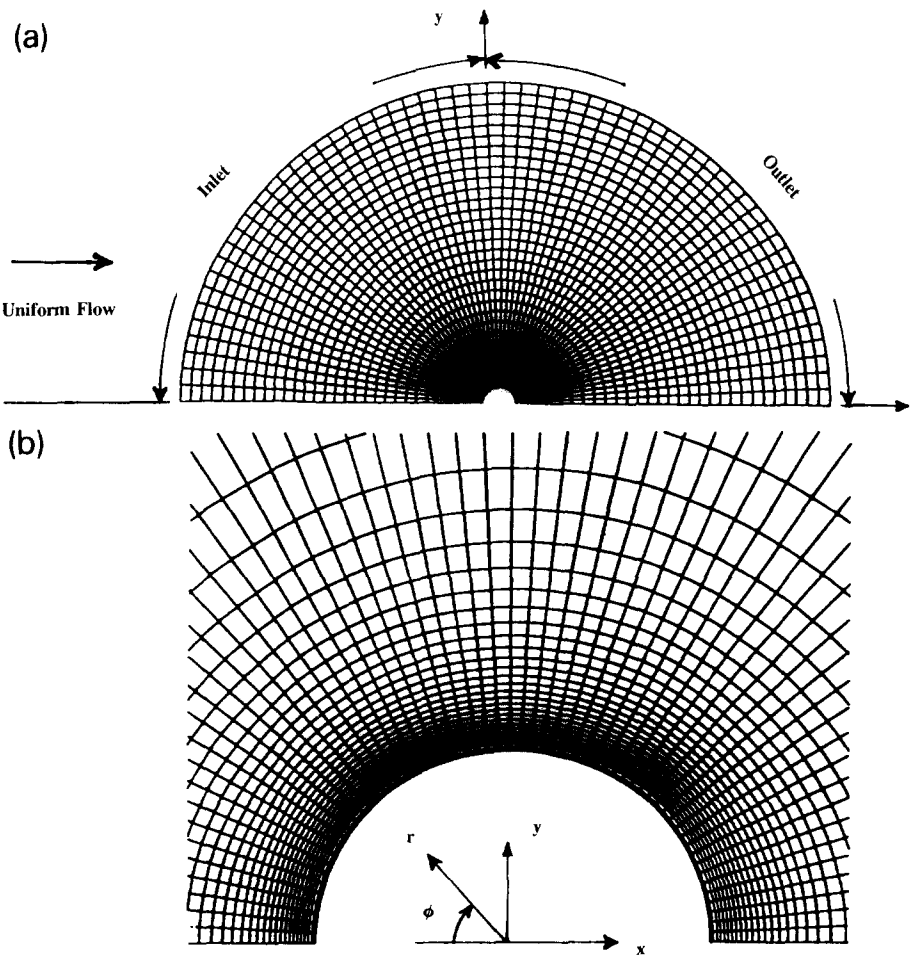

Fig. 2. (a) Example of a cylindrical-polar grid, whole domain. (b) Example of a cylindrical-polar grid, near the cylinder.

At the wall boundaries the wall function approach was used (see, e.g., Ref. [22]) with the shear stress calculated from the log-law. The wall values of k and ε were set at the first grid node inside the calculation domain according to

$$k = u_*^2/\sqrt{C_\mu}, \quad \varepsilon = \frac{C_d k^{3/2}}{\kappa y_w} = \frac{u_*^3}{\kappa y_w}, \tag{5}$$

where $u_* = \sqrt{\tau_w/\rho}$ is the friction velocity, and y_w is the normal distance from the wall. In some calculations the generalized wall functions (see Ref. [24]) were also used. This did not produce any significant changes in the solutions.

For mean flow calculations the only parameter that is of importance, as far as the turbulence is concerned, is the eddy viscosity, rather than the actual values of the

turbulent kinetic energy, k, and its dissipation rate, ε. Hence, we conclude that the wall boundary conditions imposed on k and ε using the log-law should have no particular significance concerning the mean flow predictions when $y^+ < 11.5$, which is an empirical cutoff value beyond which the log-law is assumed to be valid.

2.3. Grid distribution

Cylindrical-polar grids were used to allow the desired distribution of grid points very close to the cylinder surface and to overcome the problems inherent to generalized BFC grids (see Ref. [25] for a discussion).

The grid points were spaced in proportion to the magnitude of the potential flow velocity gradients. Outside the boundary layer and upstream of the separation point, the velocity gradients are reasonably approximated by the potential flow theory. This fact is used to distribute the grid in the radial direction at equal increments of azimuthal velocity. A consequence of this method is that it gives large radial cell widths far away from the cylinder hence leading to large grid aspect ratios. To avoid this, the cell width is set to a constant (a fraction of the cylinder radius between 0.5 and 1) when the potential flow distribution method gave a larger cell width. Within the boundary layer the velocity gradients are much higher and spacing the grid at equal velocity increments would produce large cell aspect ratios. This is undesirable because high cell aspect ratios can lead to problems with numerical diffusion and convergence. To reduce the cell aspect ratio the number of tangential grid lines would have to be increased to an unreasonably high value. To avoid these problems, the grid within a distance of 2% of the cylinder diameter is distributed to keep the radial cell expansion ratio equal to 2. The region within 2% of the cylinder diameter is identified as the boundary layer region. This was chosen as a typical boundary layer thickness near the separation point for Reynolds numbers in the range of 10^5 to 10^7 [26]. In the azimuthal (ϕ) direction, the grid was distributed with equal spacing.

For this study, two potential flow grid distributions were tested outside the boundary layer region. The first grid distribution, GRID1 has grid points in the radial direction spaced at 5% changes in azimuthal velocity. The cell width is set equal to the cylinder radius if a 5% change in velocity gives a larger cell width. This gives a total of 35 cells in the radial direction. The grid is spaced uniformly in the azimuthal direction with 40 cells.

The second grid distribution, GRID2 is similar to GRID1 but the grid is made 50% finer outside the boundary layer region. The grid is spaced in the radial direction at 3.33% changes in velocity with a maximum cell size of 0.67 radii. This gives 55 cells in the radial direction outside the boundary layer region. There are 60 cells in the azimuthal direction.

To investigate the effect of the grid distribution close to the cylinder surface grid points were incrementally added to the boundary layer region of GRID1 and GRID2. The grid points in the boundary layer region were distributed to yield a radial cell expansion of 2 (as described above). The number of grid points in the boundary layer region ranged from 0 to 9. A suffix, NB#, was added to the GRID1 and GRID2 names to identify the number of grid points in the boundary layer region. For

example, GRID1NB3 identifies GRID1 with 3 grid points added to the boundary layer region. An example of a cylindrical-polar grid, GRID2NB5, is shown in Fig. 2.

Finally another fine grid was generated using a uniform grid expansion ratio of 1.3 in the radial direction. This (100×150; radial by axial) grid had 25 points within 2% of the cylinder diameter from the surface with 60 cells from 0° to 90° and 90 cells from 90° to 180°. The smallest cell had a radial height of 6.67×10^{-6} times the cylinder diameter. Such a small cell size was selected to approximately match the smallest cell size used by Ishii et al. [8].

2.4. Calculation domain

Because of the elliptic nature of the flow considered, in particular the pressure distribution being governed by a Poisson equation, and also because of the boundary conditions not being well defined at the open (free) boundaries, the numerical solutions are very sensitive to the relative size of the calculation domain. A systematic investigation of the domain influence [23] showed that a calculation domain extending to $r = 10d$ was adequate to minimize this effect. This domain size, which was used in the present calculations, is the same as that used by Majumdar and Rodi [1]. It is also close to that used by Ishii et al. [8] which extended from $-8.5d$ to $18D$ in the streamwise direction and from 0 to $8.5d$ in the y-direction.

2.5. Convergence

Convergence was found to be rather slow with the iteration procedure employed for the present simulations. This was particularly true for grid distributions with cells close to the wall ($5 < y^+ < 20$) where the dissipation rate, ε, is large. Larger cell aspect ratios also seemed to cause convergence problems. After extensive experiments with relaxation factors it was found that false time step relaxations close to the Courant limit [20] gave the fastest convergence rate for most grids.

Three criteria were monitored to determine if a case is converged: (i) the relative residuals (ratio of the absolute residual to the total flux of a property into computational domain) of pressure and velocities had to be less than 0.1%, (ii) the property values at a grid point in the boundary layer just past the separation point could not change significantly over a large number (> 500) of iterations, (iii) the change in the pressure coefficient over $0^\circ < \phi < 180^\circ$ is negligible over a large number of iterations. For most cases these criteria were exceeded considerably. The actual values of the residuals for typical cases can be found in the report by Celik and Shaffer [23].

2.6. Laminar bench-mark cases

First fully laminar flow simulations were performed to validate the overall calculation procedure and to ensure correct implementation of the code. The predicted pressure coefficient around the cylinder was compared with the experimental data (see Ref. [25]) of Grove et al. [27] for a Reynolds number of $\mathrm{Re} = 40$; an excellent agreement was found between the two. Another laminar flow measurement by Shaffer

[28,29] at a Reynolds number of 2000 was simulated. Here the actual flow was unsteady due to the vortex shedding. Experiments [6,29] have shown that the flow becomes turbulent in the wake at this Reynolds number. The transition occurs between 1 to 3 diameters downstream of the cylinder center. However, this should not significantly affect the mean flow around the cylinder. This case was simulated with a BFC grid fitted to the exact geometry of the wind tunnel in which the measurements were made. A comparison of the long-time exposure pathline measurements [2] with our calculated streamlines showed again very good agreement. The separation point as well as the overall size of the recirculation zone is reasonably predicted. The good agreement observed for the Reynolds number of 40 and 2000 indicated that the code is reliable and is being implemented properly (see Refs. [23,25] for more details).

3. Results and discussion

3.1. Subcritical flow simulations

Simulations were performed at $Re = 1.0 \times 10^5$ as an example for the subcritical flow regime. This Reynolds number marks approximately the beginning of the critical flow regime. In this flow regime the boundary layer along the cylinder surface remains laminar up to and after the separation point. The flow becomes turbulent somewhere in the wake formation region (see, e.g., Ref. [6]). Unless the approaching flow is turbulent, the flow over most of the cylinder should be laminar. For this case, simulations were performed with a fully laminar model, a model with a transition to turbulence imposed just after the calculated separation point, and a fully turbulent model.

Majumdar and Rodi's [1] and our predicted pressure distributions are compared with three sets of experimental data [11,14,30] in Fig. 3. Here, the experimental data

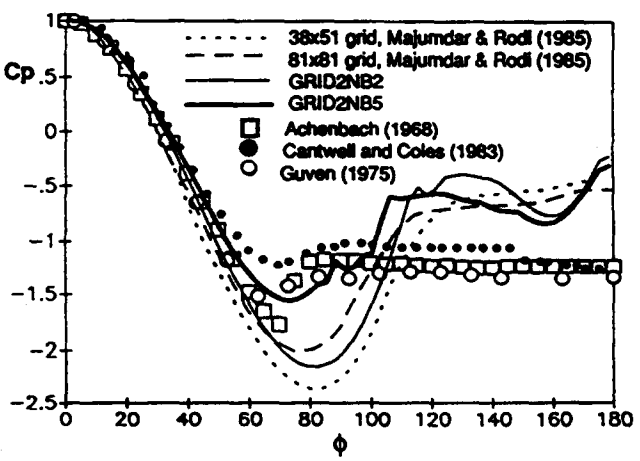

Fig. 3. Experimental and predicted pressure coefficient profiles for the subcritical regime. All predictions are for a Reynolds number of 1.0×10^5.

have not been corrected for blockage to stress the point that comparison with experiments may be misleading without correction (see Fig. 6 where the same data are presented with correction for blockage). Not all the predictions using GRID1 and GRID2 are shown here; only representative examples are shown.

It is obvious that the experimental data from various sources differ significantly for about the same Reynolds number, namely, 1.0×10^5 [11], 1.4×10^5 [14], and 2.0×10^5 [30]. Furthermore, the data do not show a trend corresponding to the Reynolds number. This of course, is due to many factors which are not identical in the experiments. For example, the blockage ratio (width of the tunnel/cylinder diameter) was 17.75%, 3.32%, and 16.67% for Achenbach's, Cantwell and Coles', and Guven's experiments, respectively.

It is also seen from Fig. 3 that the predictions are very sensitive to the grid distribution in the boundary layer – the predictions can be changed drastically just by adding a few grid points closer to the cylinder surface. Notice that the only difference between GIRD2NB2 and GRID2NB5 is three grid points in the boundary layer region. The distance of the first grid point from the cylinder for GRID2NB2 is 0.5% of the cylinder diameter. For GRID2NB5 the distance of the first grid point is 0.065% of the cylinder diameter. Our predictions with GRID2NB5 show fairly good agreement with the experimental data up to and including the separation point (see also Fig. 10). Adding two or four more points (GRID2NB7, GRID2NB9) closer to the cylinder surface did not significantly change the predictions. The grid dependence between Majumdar and Rodi's 38×51 and 81×81 predictions is also noteworthy. Their calculations were performed with transition to turbulence imposed immediately after the separation point.

In Fig. 4 the calculated wall shear stress distribution is compared with Achenbach's [11] measurements. The wall shear stress, τ_w, is made non-dimensional as $\bar{\tau}_w = (\tau_w/\rho U^2_\infty)\sqrt{\mathrm{Re}}$. Again, only representative predictions are shown here.

Results from two different grids (GRID2NB3 and GRID2NB5) illustrate the dependence of the predictions on the grid distribution in the boundary layer region. As with the pressure profile prediction, adding more grid points closer to the cylinder (e.g., GRID2NB7, GRID2NB9) did not change the prediction obtained with GRID2NB5. For GRID2NB5 the wall shear stress was calculated with two different approximations of the radial gradient of the azimuthal velocity, du/dy. First, du/dy is approximated by a linear fit through the first two grid points. Then, it is approximated by a cubic curve fit through the first three grid points i.e., $u = ay + by^3$. As is shown in Fig. 4 the parabolic approximation slightly improves the agreement between predictions and the experiments. The predicted separation angle of 80° matches (within experimental uncertainty) the experimental value of 78°. It is noteworthy that Majumdar and Rodi [1] with their transitional model predicted a separation at 89° with their 81×81 grid. Judging from our results, this could be due to placing the first grid point too far from the cylinder surface. This could not be verified, however, since Majumdar and Rodi did not report their exact grid specifications.

Beyond the separation point the predictions differ significantly from the experiments and the fully laminar flow predictions oscillate. The predicted velocity fields show multiple zones (see Fig. 5) associated with these oscillations as evidenced by the

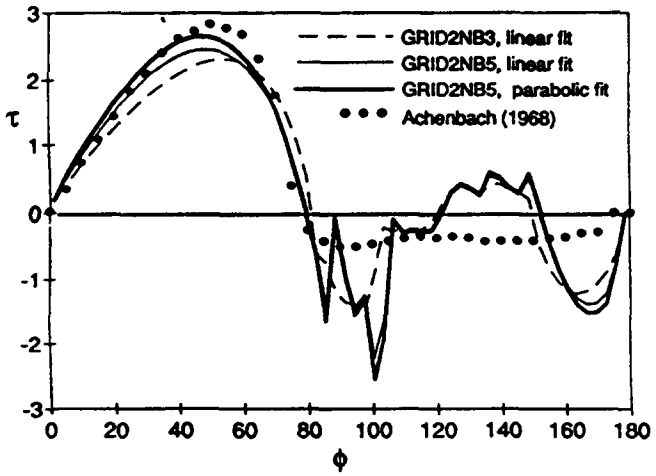

Fig. 4. Comparison of predicted and experimental wall shear stress data for a Reynolds number of 1.0×10^5.

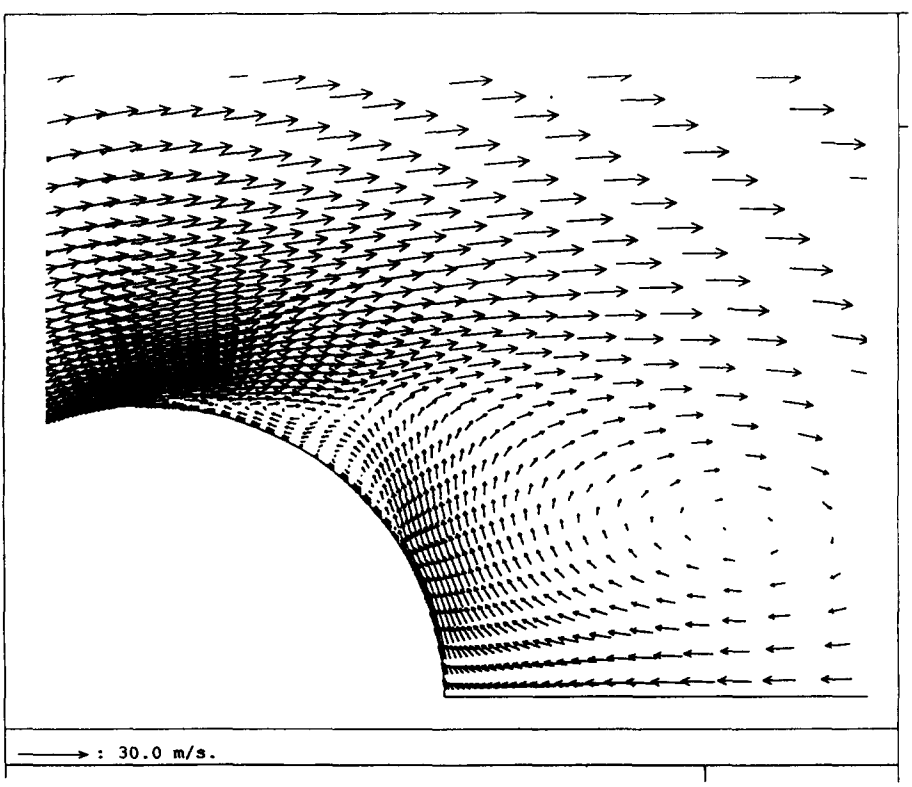

Fig. 5. Predicted velocity distribution illustrating multiple eddies, Re = 1.0×10^5.

change in sign of the wall shear stress. The authors do not know at this stage whether this represents some type of critical flow behavior or if it has any real significance. However, Ishii et al. [8] did report shear stress calculations which showed a very similar behavior to that shown in Fig. 4. Tamura et al. [12] also reported on multiple recirculation zones (eddies) similar to those shown in Fig. 5 in their calculations with no turbulence model. Their calculations showed that the number of the eddies increased and the location of separation moved upstream as they made the grid spacing finer and finer. The predictions of Majumdar and Rodi do not show this oscillatory behavior. This could be due to their imposition of transition to turbulence after the separation point.

To test this hypothesis we applied our transitional model to the same case. However, along with the transition phenomenon we had to reconsider grid dependence under the guidance of the Tamura et al.'s calculations which showed continuous dependence on grid fineness. The blockage effects were also considered in detail. In what follows these issues are addressed one by one.

3.2. *Blockage effects*

Most simulations presented in the literature for flow past circular cylinders are without any blockage, i.e. the cylinder is in a uniform flow without any tunnel walls. Experiments, on the other hand, are performed in tunnels with finite blockage. To account for this, the experimental pressure data were corrected for blockage using the semi-empirical formula suggested by Allen and Vincenti and later modified by Farell et al. [31]. This procedure gives a good estimate for blockage effects in agreement with experimental observations of Richter and Naudasher [32]. Without blockage the minimum pressure coefficient, C_{pm}, and the base pressure coefficient, C_{pb}, decrease in absolute value. This, as expected, results in a decrease in the drag coefficient. When predictions are compared with corrected pressure distributions the observed "good agreement" may deteriorate. Hence, in the rest of the presentation the experimental data were corrected for blockage whenever possible before comparing them with predictions. The influence of tunnel blockage can be seen by comparing the experimental data presented in Figs. 3 and 6 without and with correction, respectively. The experimental data from different sources collapses to a narrower band when corrected for blockage, and the agreement that is seen in Fig. 3 between predictions and measurements indeed deteriorates.

3.3. *Influence of transition*

Fig. 6 shows the predicted pressure distribution for a Reynolds number of 1.0×10^5 with transition imposed at various locations. The location of the transition, ϕ_{tr}, shown in Fig. 6 indicates the middle of the transitional region. The experimental data used for comparison have been corrected for blockage. The collapse of the data to a narrower band after blockage correction is noteworthy. The location of the transition has a significant influence on the pressure distribution as its is seen in Fig. 6. The predictions exhibit a significantly different flow behavior compared to that of the

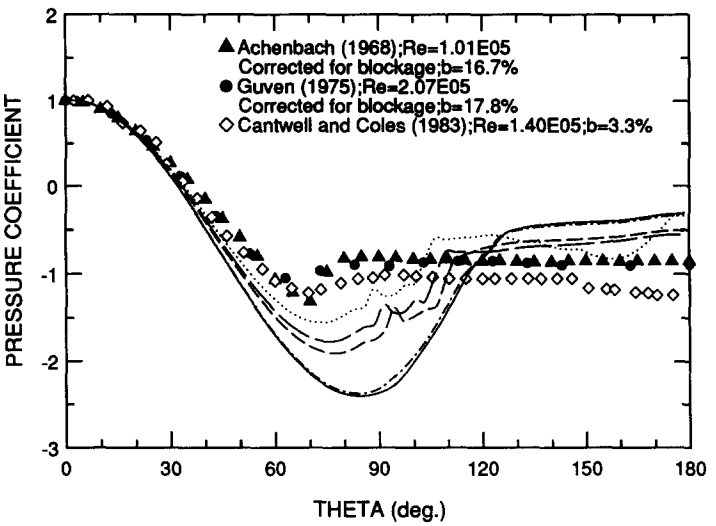

Fig. 6. Pressure distribution. Predictions: present work; $Re = 1.0 \times 10^5$; (—) tr6nb5a, $\phi_{tr} = 99°$; (– – –) tr6nb5b $\phi_{tr} = 114°$; (–·–·–) tr6nb5c $\phi_{tr} = 93°$; (— —) tr6nb5d $\phi_{tr} = 125°$; (...) lam6nb5.

experiments. When the transition is between 90° to 110° the predicted flow shows a supercritical behavior, when it is beyond 110° it shows a critical flow behavior. Comparison of the fully laminar flow calculations (case lam6nb5) with others indicates that even if the transition is imposed after the separation point it still greatly affects the pressure distribution in the upstream region. With transition, the magnitude of the base pressure increases leading to a better agreement with experimental data.

The calculated skin friction distributions with the transitional model are shown in Fig. 7. When ϕ_{tr} is beyond 110° the location of the laminar separation is predicted correctly at 82.50°. The imposed transition to turbulence causes the flow to reattach thus forming the so-called "laminar-separation-turbulent reattachment bubble". This is apparent from the relatively flat region on the pressure distribution curve (Fig. 6, case tr6nb5b and case tr6nb5d) between 90° to 100° as well as from the sign changes in the friction coefficient in Fig. 7. Hence, these predictions do simulate an experimentally observed phenomenon (see also Fig. 9) but at an effectively lower Reynolds number compared to the experiments. When the transition point corresponds to a location upstream of the separation point, i.e. supercritical flow regime, this manifests itself by a sudden increase in the wall shear stress as it is depicted in Fig. 7 (case tr6nb5a, tr6nb5c). This is also an experimentally observed phenomenon as it is illustrated qualitatively in Fig. 8. Here, the transition to turbulence was enhanced by the free stream turbulence, Tu = 0.9%, in the experiments at a Reynolds number of 4.45×10^5. This suggests that, probably due to the relatively coarse grid used, the present calculation produces a solution at an effectively large Reynolds number than the imposed one. This may be caused by the influence of the high artificial viscosity inherent to the numerical scheme used in the present calculations. This point shall be

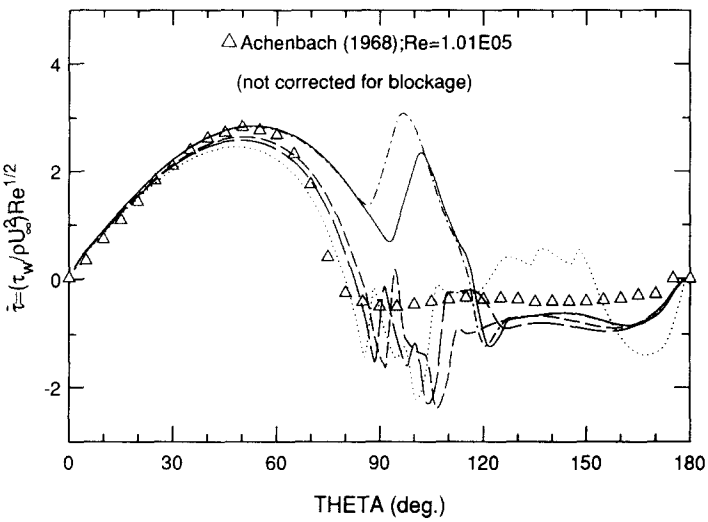

Fig. 7. Skin friction distribution. Predictions: present work; $Re = 1.0 \times 10^5$; (——) tr6nb5a, $\phi_{tr} = 99°$; (– – –) tr6nb5b $\phi_{tr} = 114°$; (– · – · –) tr6nb5c $\phi_{tr} = 93°$; (— — —) tr6nb5d $\phi_{tr} = 125°$; (···) lam6nb5.

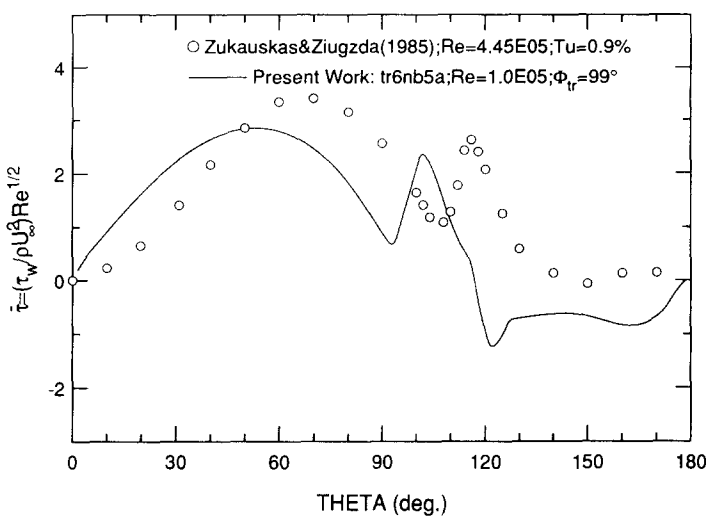

Fig. 8. Illustration of transition of turbulence prior to flow separation.

investigated further by decreasing the grid size. However, before that, we illustrate the sensitive nature of the flow in this Reynolds number range by referring to another set of experiments, namely that of Fage and Falkner [32].

Fig. 9 shows several pressure distributions measured by Fage and Falkner [33] at Reynolds numbers close to $Re = 1.0 \times 10^5$ along with predictions with transitional

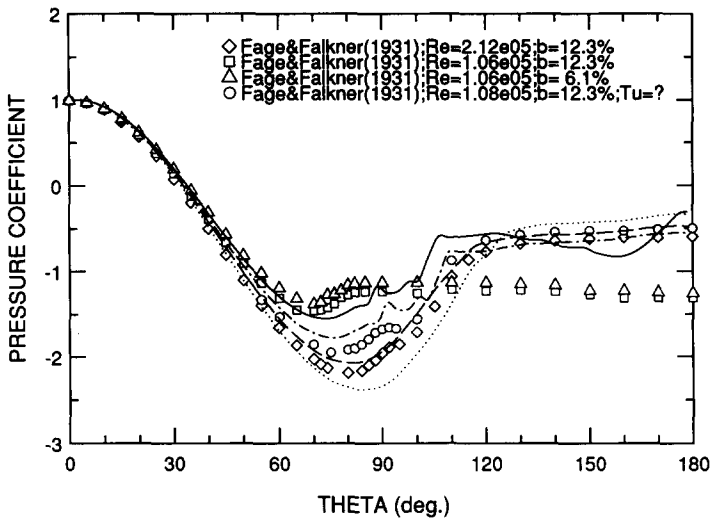

Fig. 9. Pressure distribution; present work; Re = 1.0×10^5; (——) lam6nb5; (– – –) tur6nb5; (···) tr6nb5cv; (–·–·–) tr6nb5dv.

(cases tr6nb5cv, $x_{tr} = 0.026d$; tr6nb5dv, $x_{tr} = 0.3d$), fully laminar (case lam6nb5), and fully turbulent calculations (case tur6nb5). The experiments show the significant effects of the Reynolds number and free stream turbulence on the flow regime in this Reynolds number range. Increasing the Reynolds number from 1.06×10^5 to 2.12×10^5 causes the flow to switch from the subcritical to supercritical regime. Introducing some turbulence to the approaching stream, via thin ropes in this case, at Re = 1.08×10^5 results in a critical flow regime with the reattachment bubble present. Another case with a blockage ratio of 6.1% as opposed to 12.3% for the other cases shows the influence of blockage which seems not to be so large for these experiments. It is interesting to note that at Re = 1.0×10^5 all three flow regimes can be produced numerically by simply manipulating the location of transition in the model. This confirms the assertion that the flow is very sensitive to any disturbances in this Reynolds number range. The occasionally obtained good agreement between experiments and predictions in this figure may also be deceiving as it shall be illustrated next by using a finer grid distribution.

3.4. *Fine grid solution*

Fig. 10 shows the calculated pressure distribution in comparison with experiments for the same Reynolds number as before (Re = 1.0×10^5) but with a much finer grid of 100×150 (y-, x-directions) described in Section 2. Comparison of this figure with Fig. 6 shows the significant grid dependence of previous calculations. The experimental data is bounded by the fully turbulent and the fully laminar calculations except for the base pressure coefficient. A good agreement is obtained with the transitional

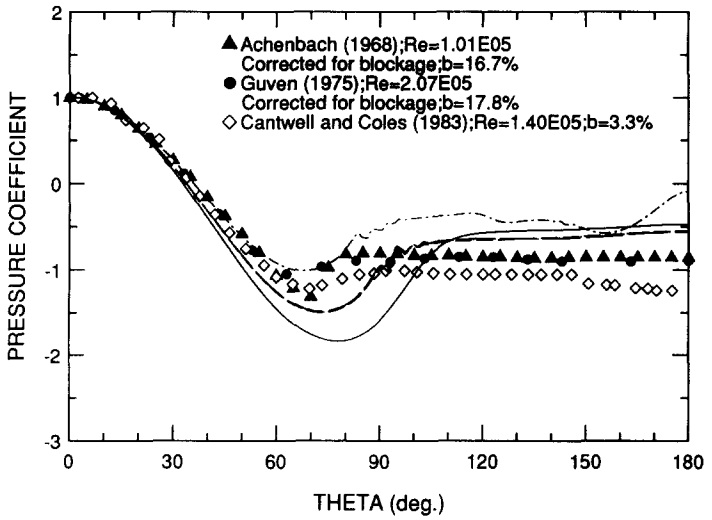

Fig. 10. Pressure distribution; Re = 1.0×10^5; predictions: present work (100×150 grid); (– – –) tran125 (···) tran140; (— —) tran170; (——) full turb; (– · · · –) fullam.

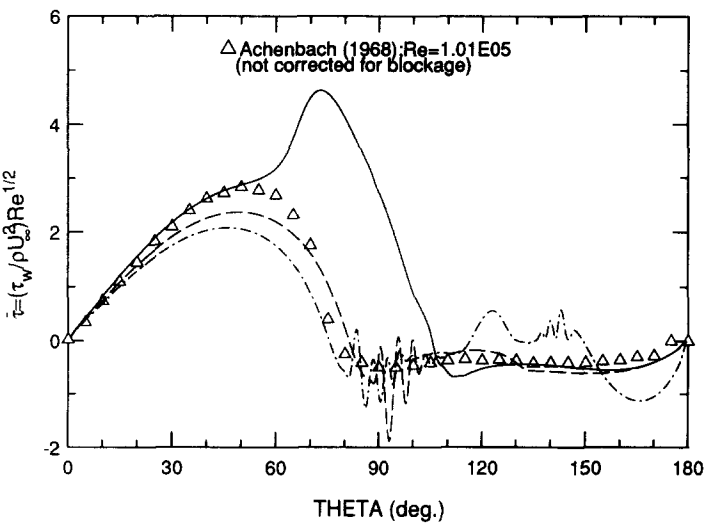

Fig. 11. Skin friction distribution; Re = 1.0×10^5. Predictions; present work (100×150 grid; (——) fullturb; (– – –) tran 125; (– · – · –) fullam.

model with $\phi_{tr} > 110°$. The significant improvement in the predicted base pressure coefficient with transition is noteworthy. The corresponding skin friction distribution is presented in Fig. 11. Here the focus should be on the shapes and sign changes rather than the actual magnitude because the wall shear stress, τ_w, is indirectly approximated

from calculated velocity profiles. Nevertheless, this figure shows that with the transitional model the location of the separation is predicted at 82° in close agreement with experiments. The oscillations seen in the wake region with the fully laminar model are suppressed to a large extent when the transition is imposed. These oscillations, which are not seen in measurements, were also present in the time averaged skin friction distributions presented by Ishii et al. [8] from their unsteady, two-dimensional calculations with no turbulence model. It seems that these are the results of instabilities arising from the intermittent characteristic of the transitional flow immediately after separation. The experiments indicate a fully turbulent flow in this region without any oscillations in the τ_w distribution. When the fully turbulent flow model is used, the predictions do not show such oscillations.

One other interesting feature of the fine grid solution with the fully turbulent model is the sudden increase in τ_w around $\phi = 70°$. This indicates a fairly sharp transition from laminar to turbulent flow in the boundary layer as it is seen in Fig. 12 from the dimensionless eddy viscosity variations. For these calculations the first point was at about 0.015% of the cylinder diameter from the surface. The calculated eddy viscosity at this point was less than the laminar viscosity (see Fig. 12). It is interesting to note that a transition to turbulence is predicted in both axial and radial directions as it is depicted in Fig. 12.

3.5. *Comparison with other calculations*

In Figs. 13 and 14 we present a comparison of previous computations from the literature with each other, as well as with experiments and our own calculations. The

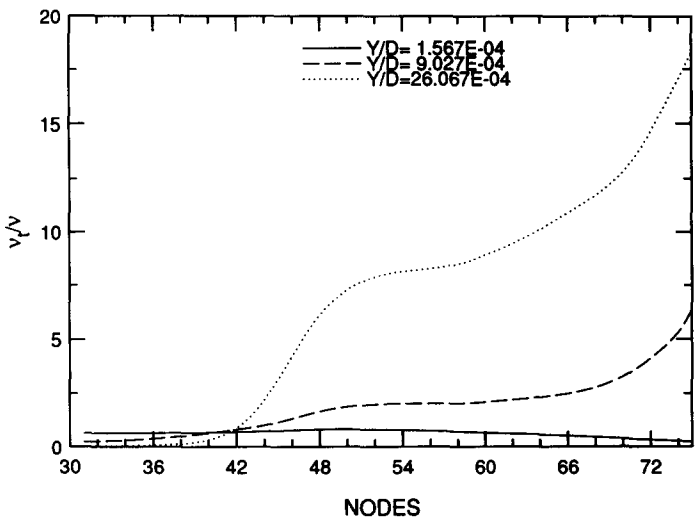

Fig. 12. Calculated turbulent eddy viscosity distribution in the boundary layer; Re = 1.0×10^5 (100×150 grid).

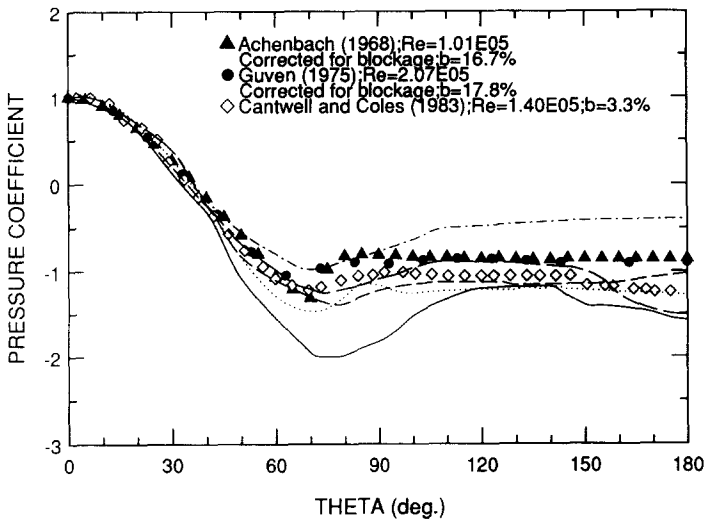

Fig. 13. Pressure distribution. $Re = 1.4 \times 10^5$; prediction: (– – –) 3D LES; (——) 2D PLES [19]; (— — —) 2ZLRR; (– · – · –) 2Z$k\varepsilon$ [18]; (· · ·) 2D PLES [13].

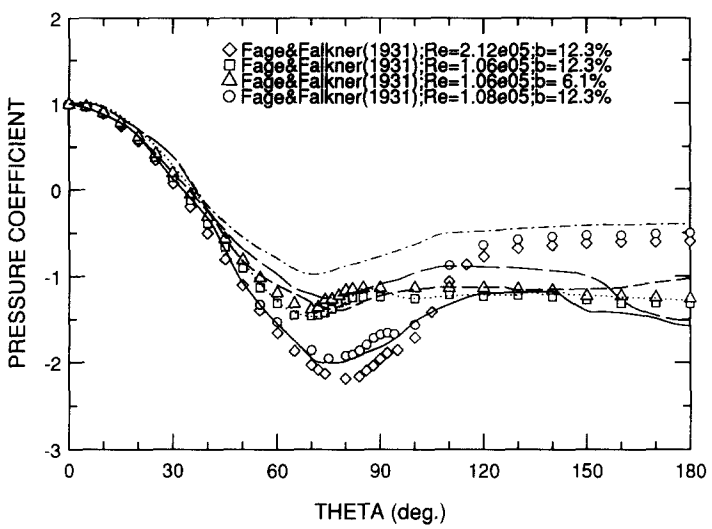

Fig. 14. Pressure distribution. $Re = 1.4 \times 10^5$; predictions: (– – –) 3D LES; (——) 2D LES [19]; (——) 2ZLRR; (– · – · –) 2Z$k\varepsilon$ [18]; (· · ·) 2D LES [13].

references cited in these figures are discussed in Section 1.2 and a summary is given in Table 1.

Fig. 13 shows the comparison of previous computations with various experimental data corrected for blockage. Franke's [18] predictions with the two-zone k–ε model

resembles our predictions with the fully laminar model. The predictions by Franke were obtained by time averaging from unsteady, two-dimensional calculations. In this respect they should account for the influence of vortex shedding phenomenon. It is surprising to see that the predicted base pressure is still too low in absolute value. The two-zone Reynolds stress transport model predictions (2ZLRR) of Franke seem to give a better agreement with experiments except in the vicinity of the rear stagnation point. Here, an unexpected increase is observed in the magnitude of the calculated base pressure. The pseudo-LES of Kato and Ikegawa [19] does not predict the subcritical nature of the flow; the base pressure is too high contrary to all other calculations. The reader is reminded that Kato and Ikegawa's calculations are for $Re = 1.0 \times 10^4$ and include some ad hoc transition criteria in the direction normal to the cylinder surface. Their full 3D LES results are in good agreement with experiments except for the base pressure which is relatively large. The two-dimensional pseudo-large-eddy simulations (2D PLES) of Song and Yuan [13] are as good as the 3D LES by Kato and Ikegawa. Intuitively, these calculations should give significantly different results (see for example 2D versus 3D calculations presented by Tamura et al. [12]). An explanation to this may be found in different ways of handling the boundary layers, and the different subgrid coefficients used in the Smagorinsky model. The particular grid distribution used by each investigator may also play a role.

In Fig. 14 the computations presented in Fig. 13 are compared with another set of experiments [33]. This figure also confirms the good agreement obtained with the 3D LES [19] and the 2ZLRR model predictions [18]. The 2D PLES of Kato and Ikegawa seems to result in a critical flow regime like our own calculations with a course grid (see Fig. 12) which indicates that these calculations are most probably grid dependent.

In Fig. 15 we compare our fine grid simulations with the fully laminar and the transitional model with other computation. It is seen that our 2D steady calculations are in good agreement with the 3D LES of Kato and Ikegawa, and the 2ZLRR model predictions of Franke. Our calculations predict a relatively low base pressure coefficient in magnitude compared to the others. However, we cannot say that this is because of the fact that we did not account for the effects of the unsteady vortex shedding. The 2D unsteady calculations with the $2Zk$–ε model by Franke do also produce low base pressure coefficient.

3.6. *Supercritical flow simulations*

Simulations were also performed for a fully turbulent flow at a Reynolds number of 3.6×10^6. This case was experimentally investigated by Achenbach [11]. He used a pressurized wind tunnel with a blockage ratio of 17.75% and a free stream turbulence intensity less than 0.7%. The measured pressure distribution (Fig. 16), separation angle, and drag coefficient all indicate a supercritical flow. According to Achenbach, in his experiments the critical flow regime covered a range of $3 \times 10^5 < Re < 1.5 \times 10^6$. In Fig. 16, representative calculated pressure distributions from this work and from the literature are compared with Achenbach's experimental data. In this figure both corrected and uncorrected pressure coefficients for blockage

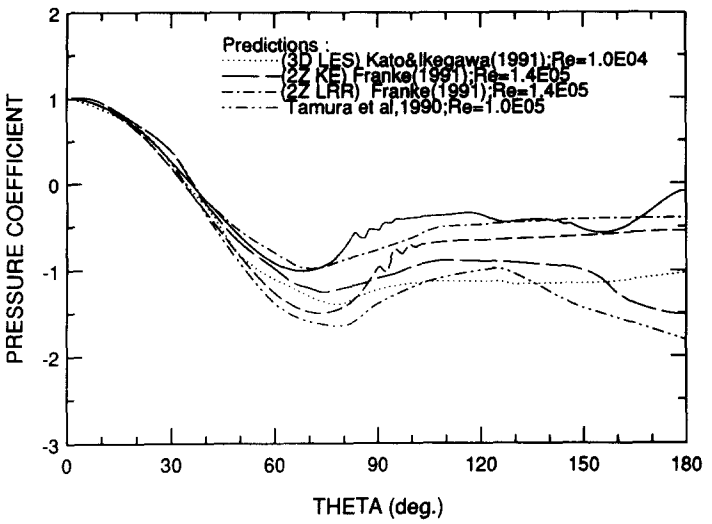

Fig. 15. Pressure distribution. Present work (100 × 150 grid); Re = 1.0×10^5; predictions: (——) fullam; (– – –) tran 125.

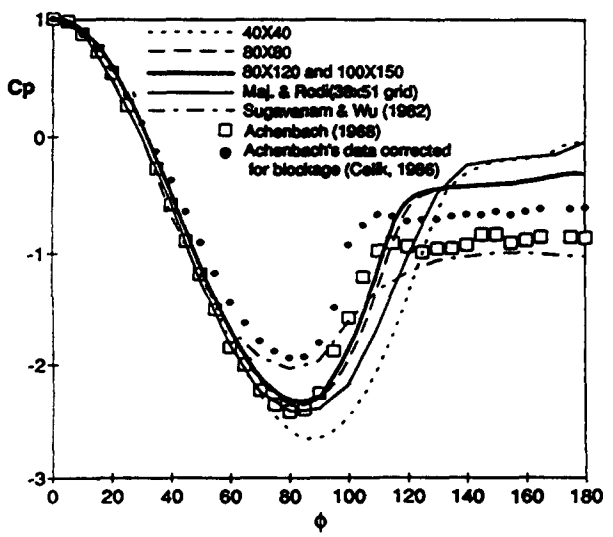

Fig. 16. Predicted and experimental pressure coefficient data for supercritical flow at a Reynolds number of 3.6×10^6.

are depicted for comparison. Predictions with the 40 × 40 grid show similar characteristics to Majumdar and Rodi's predictions with their 38 × 51 grid. Simulations with finer grids (80 × 80, 80 × 120 and 100 × 150) improve the predictions significantly as shown in Fig. 16. With the 80 × 120 and 100 × 150 grids, the separation angle is

predicted at 118°. This is in good agreement with the measured value of 115°. The predictions with the 100×150 grid were practically the same as those with the 80×120 grid. This indicates that the predictions with the 100×150 grid are most probably grid independent. The significant improvement in the prediction of the base pressure compared to the previous predictions is noteworthy. However, there is still a significant difference between the measured and calculated base pressures. As suggested by Majumdar and Rodi, one reason may be that the model does not account for the effects of vortex shedding. Another contributing factor may be the well-known shortcomings of the standard k–ε turbulence model in predicting separated flows with strong adverse pressure gradients [34].

An important difference between the 100×150 grid simulations and the coarser 40×40 grid simulations is the location of the first grid point. For the 100×150 grid the y^+ value at the first grid point ranged from 2 to 18 from $\phi = 0°$ to 180°. For the 40×40 grid the y^+ value ranged from 11 to 81 from $\phi = 0°$ to 180°. Depending on the way the shear stress is calculated these y^+ values can be smaller by about a factor of 2. As mentioned earlier, when the first point is very close to the wall the usual wall boundary conditions for k and ε should not have a strong influence on conditions farther away from the wall [1]. Hence, the nearer the first grid point to the surface, the less important should be the uncertainties involved in the wall function approach as far as the mean flow predictions are concerned. Indeed, this seems to be the case in the present simulations.

Sugavanam and Wu [9,10] have published predictions showing exceptional agreement with Achenbach's experimental data (as it appears in their paper). However, Majumdar and Rodi [1] questioned Sugavanam and Wu's predictions. The present authors agree with Majumdar and Rodi. We duplicated Sugavanam and Wu's grid but our predictions were quite different from theirs. This is perplexing because the turbulence model and the wall functions are essentially the same. Furthermore, our studies indicate that the 20 cells used by them in the azimuthal direction are far too few to produce a grid independent prediction.

Fig. 17 compares the measured and the calculated wall shear stress, τ_w, distribution. It is seen that the measurements are not symmetric on the two sides of the cylinder. This is characteristic of the flow regime in the critical flow regime. It is not clear whether the supercritical flow regime is fully established at this Reynolds number. The predictions with the standard wall functions over predict the shear stress by a factor of 3. The maximum dimensionless shear stress is predicted as 13.7 at 70°. The flow separation is predicted at 117°. The measured τ_{max} is about 4 at 65°, and ϕ_s is 115°. Our predictions are comparable to Majumdar and Rodi's predictions (not shown here) with the 38×51 grid. They reported a maximum dimensionless shear stress of 11.25 at or about 65°. Since for the fine grid solution the first grid was in the sublayer or at most in the buffer layer, we calculated the shear stress also from $\tau = \mu(du/dy)$. The derivative of the velocity was approximated from the first two grid points. This is consistent with the velocity being proportional to the distance, y, from the wall within the sublayer. The shear stress calculated from the derivative of the velocity was not significantly different than the one calculated from the log-law.

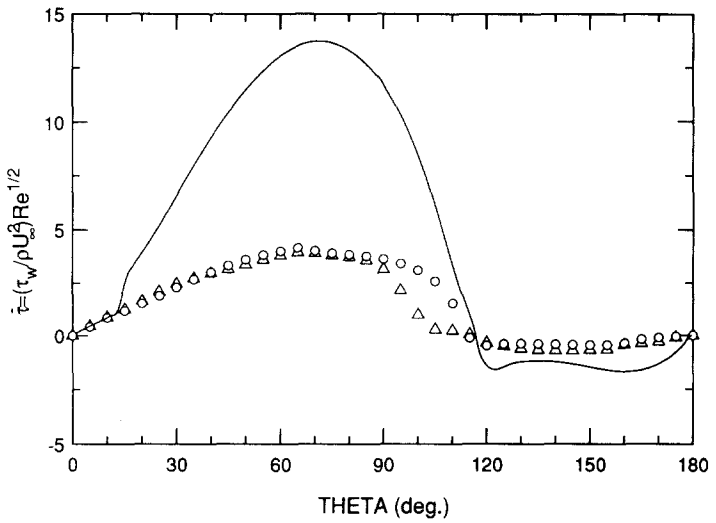

Fig. 17. Skin friction distribution. Re = 3.6×10^6; without wall damping (——).

3.7. *Pressure gradient effects*

It is well known (see e.g., Ref. [26]) that the boundary layer around a circular cylinder does not exhibit a state of local equilibrium, i.e., the production of turbulent kinetic energy, k, is not equal to its rate of dissipation, ε. This is especially true near the separation point. The deviation of velocity profiles from that of the equilibrium boundary layers as a result of pressure gradient effects was investigated by Patel [35]. He proposed a modified log-law which explicitly includes the pressure gradient as a parameter. Since most of the discrepancies between the predictions and the measurements are seen in the adverse pressure gradient region, it is plausible that using Patel's wall function formulation should improve the predictions. Preliminary calculations of the wall shear stress using Patel's function did indeed indicate this. However, at the time of this report a careful study had not been completed – a full implementation of the new wall function is necessary before reaching a definite conclusion. An alternative way of accounting for the pressure gradient effects is to use a one-equation turbulence model [34] in the near wall region as suggested by Patel [36]. This approach employs a prescribed mixing length distribution which does not seem to be affected by the pressure gradient.

3.8. *Wall damping of* v_t

In some calculations (see, e.g., Refs. [13,19]) the eddy viscosity, v_t, is modified in the vicinity of the wall to account for wall damping. This was also investigated by us. Our predictions (not shown here) like those of the above authors with wall damping gave excellent agreement between predicted and measured pressure distribution at

$Re = 3.6 \times 10^6$ and $Re = 8.4 \times 10^6$. However, a close examination of the velocity profiles in the boundary layer revealed unreasonable multiple inflection points prior to separation. For this reason, we did not include these predictions in this paper, but they can be found in a report by Celik and Shaffer [23]. Since the other authors did not present details of the velocity profiles, it is not possible to access their results from this perspective.

4. Conclusions

The mean turbulent flow past "smooth" circular cylinders is analyzed using a readily available Navier–Stokes solver. Attention was focused on subcritical and supercritical flow regimes. For the subcritical flow regime, fairly good agreement can be obtained up to and including the separation point between experiments and predictions with the transitional model. This is contingent on having a sufficient number of grid points placed in the thin boundary layer of the cylinder. After the separation point agreement between predictions and experimental data is not so good. This could be attributed to the fact that the model does not account for the presence of vortex shedding, the influence of which should be seen immediately after the separation point. However, predictions from the literature including unsteady vortex shedding do not indicate a significant improvement in this region. Other effects such as surface roughness and the presence of an adverse pressure gradient are probably important.

For the supercritical flow predictions, we found that the pressure distribution, and the location of separation can be predicted in fairly good agreement with measurements. But, the wall shear stress is over predicted with unreasonably high values. This should be the result of the actual distribution of the turbulent eddy viscosity in the boundary layer. As with the subcritical case, the predictions are strongly influenced by the grid distribution in the boundary layer. Our best predictions are achieved when the first grid point is placed within the viscous sublayer.

In all cases a lower pressure coefficient in absolute value is predicted compared to experiments. Considering only mean flow quantities, it has been found that when carefully applied, and the grid is distributed properly, the long time-averaged solutions using the standard k–ε model with a transition criteria are as good as those of more expensive models. A true comparison with large-eddy simulations cannot be made because the only three-dimensional transient LESs known to us was performed at $Re = 1.0 \times 10^4$ with ad hoc transition criteria in the boundary layer. Furthermore, in these calculations grid dependency was not investigated.

Finally, there is some incertitude when simulations are evaluated using the experimental data presented in this paper. For example, to draw definite conclusions the exact experimental conditions, including the tunnel blockage and the surface roughness, must be simulated. This, of course, is not always possible. We suggest that in addition to evaluation by experimental data, predictions be compared with bench mark cases produced by direct or by strictly large eddy simulations.

Acknowledgement

The authors wish to express their gratitude to Jim Hickerson, Jim Ekmann and Dr. Mahendra Mathur for motivating and supporting this work. This work was sponsored by the U.S. DOE Pittsburgh Energy Technology Center in conjunction with the Oak Ridge Associated Universities Part Time Faculty Participation Program.

References

[1] S. Majumdar and W. Rodi, Numerical calculation of turbulent flow past circular cylinders, in: Proc. 3rd Symposium on Physical aspects of aerodynamic flows, Long Beach, California, 21–24 January, 1985.
[2] I. Celik, Analytical modeling of the mean flow around circular cylinders: A Review, in: Proc. ASCE Specialty Conference on Advancements in aerodynamics, fluid mechanics, and hydraulics, Minneapolis, 3–6 June, 1986.
[3] I. Celik and F.D. Shaffer, Calculation of the mean flow past circular cylinders using a Navier–Stokes Solver, U.S. DOE Technical Report, Pittsburgh Energy Technology Center, Pittsburgh, PA (1994).
[4] C. Farell and J. Blessman, On critical flow around circular cylinders, J. Fluid Mech. 136 (1983) 375–391.
[5] E. Achenbach, Influence of surface roughness of the cross-flow around a circular cylinder, J. Fluid Mech. 46 (1971) 321–335.
[6] S.M. Bloor, The transition to turbulence in the wake of a circular cylinder, J. Fluid Mech. 19 (1964) 291–304.
[7] S. Szepessy, On the three-dimensionality of vortex shedding from a circular cylinder, Ph.D. Dissertation, Department of Thermo and Fluid Dynamics, Chalmers University of Technology, Göteborg (1991).
[8] K. Ishii, K. Kuwahara, S. Ogawa, W.J. Chyu and T. Kawamura, Computation of flow around a circular cylinder in a super critical regime, AIAA 18th Fluid Dynamics, Plasmadynamics and Lasers Conf., Cincinnati, Ohio, 16–18 July, AIAA Paper 85–1660 (1985) pp. 125–132.
[9] W. Sugavanam, Numerical study of separated turbulent flow over airfoils, Ph. D. Thesis, School of Aerospace Engineering, Georgia Institute of Technology, Atlanta (1979).
[10] A. Sugavanam and J.C. Wu, Numerical study of separated turbulent flow over airfoils, AIAA J. 20 (1982) 464–470.
[11] E. Achenbach, Distribution of local pressure and skin friction around a circular cylinder in a cross-flow up to $Re = 5 \times 10^6$, J. Fluid Mech. 34 (1968) 625–635.
[12] T. Tamura, I. Ohta and K. Kuwahara, On the reliability of two-dimensional simulation for unsteady flows around a cylinder-type structure, J. Wind Eng. Ind. Aerodyn. 35 (1990) 275–298.
[13] C.C.S. Song and M. Yuan, Simulation of vortex shedding flow about a circular cylinder at high Reynolds numbers, ASME J. Fluids Eng. 112 (1989) 155–163.
[14] B. Cantwell and D. Coles, An experimental study of entrainment and transfer in the turbulent near-wake of a circular cylinder, J. Fluid Mech. 136 (1983) 321–374.
[15] A. Rosko, Experiments on the flow past a circular cylinder at very high Reynolds number, J. Fluid Mech. 10 (1961) 345–357.
[16] W.C. Reynolds, The potential and limitations of direct and large eddy simulations, in: Whither turbulence? Turbulence at the crossroads, ed. J.L. Lumley, Proc. Workshop Held at Cornell University, Ithaca, NY, 22–24 March (Springer, Berlin, 1989)
[17] P.W. Bearman, On vortex shedding from a circular cylinder, J. Fluid Mech 72 (1965) 229–241.
[18] R. Franke, Numerische Berechnung der instationaeren Wirbelabloesung hinter zylindrischen Koerpern, "Ph. D. Dissertation, Department of Civil Engineering University of Karlsruhe, Germany (1991).
[19] C, Kato and M. Ikegawa, Large eddy simulation of unsteady turbulent wake of a circular cylinder using the finite element method, in: Proc Symposium on Advances in numerical simulation of turbulent flows, First Joint ASME-JSME Fluids Engineering Conference, Portland, Oregon, 23–27 June, 1991.

[20] J.C. Ludwig, H.Q. Qin and D.B. Spalding, The PHOENICS reference manual, CHAM TR/200 (CHAM Limited, Bakery House, London, 1989).
[21] S.V. Patankar, Numerical fluid flow and heat transfer (Hemisphere, New York, 1980).
[22] W. Rodi, Turbulence models and their application in hydraulics (Book Publication of Int. Association for Hydraulic Research, Delft, 1980)
[23] I. Celik, F.D. Shaffer and Y. Yang, A numerical study of flow around two cylinders in tandem, in: Proc. 11th Australasian Mechanics Conference, eds. M.R. Davis and G.J. Walker, University of Tasmania, Hobart, Australia, 14–18 December (1992) 103–106.
[24] H.I. Rosten and J.K. Worrell, Generalized wall functions for turbulent flow, PHOENICS J. 1 (1) (1988) 81–109.
[25] I. Celik and F.D. Shaffer, Analysis of numerical simulations of mean turbulent flow past a circular cylinder, in: Proc. Forum on Turbulent flows, The First ASME-JSME Fluids Engineering Conferences, Portland, Oregon, 23–27 June, FED-Vol. 112 (1991) 153–158.
[26] I. Celik and V.C. Patel, Boundary-layer development on circular cylinders, Bound.-Layer Meteorol. 24 (1982) 281–293.
[27] A.S. Grove, F.H. Shair, E.E. Petersen and A. Acrivos, An experimental investigation of the steady separated flow past circular cylinders, J. Fluid Mech. 19 (1964) 60.
[28] F.D. Shaffer, Fluid mechanics of ash deposition, in: Proc. U.S.D.O.E. Advanced Research and Technology Development Program Review Meeting, Morgantown, West Virginia, Vol. 1 (1989) pp. 242–251
[29] F.D. Shaffer, Private communications, U.S.D.O.E. Pittsburgh Energy Technology Center, Pittsburgh, 1990.
[30] O. Guven, An experimental and analytical study of surface roughness effects on the mean flow past circular cylinders, Ph. D. Thesis, Mechanics and Hydraulics Program, University of Iowa, Iowa City (1975).
[31] C. Farell, S. Carrasquel, O. Guven and V.C. Patel, Effects of wind tunnel walls on the flow past circular and cooling tower models, J. Fluids Eng. 99 (1977) 470–479.
[32] A. Richter and E. Naudascher, Fluctuating forces on a rigid circular cylinder in confined flow, J. Fluid Mech. 78 (1976) 561–576.
[33] A. Fage and V.M. Falkner, Further experiments on the flow around a circular cylinder, Aeronautical Research Committee, London, Reports and Memoranda, No. 1369 (1931).
[34] W. Rodi and G. Scheuerer, Scrutinizing the k–e model under adverse pressure gradient conditions, in: Proc. 4th Symposium on turbulent shear flows, Karlsruhe, Germany, 12–14 September, 1983.
[35] V.C. Patel, A unified view of the law of the wall using mixing-length theory, The Aeronautical Quarterly Vol. XXIV, R. Aeron. Soc. (1973) 55–70.
[36] V.C. Patel, Private communication, Institute of Hydraulic Research, University of Iowa, Iowa City, 1991.
[37] I. Celik, V.C. Patel and L. Landweber, Calculation of mean flow past circular cylinders by viscous inviscid interaction, J. Fluids Eng. 107 (1985) 218–223.
[38] A. Zukauskas and J. Ziugzda, Heat transfer of a cylinder in cross flow (Hemisphere, New York, 1985).

Appendix A

Equations for the standard k–ε model

k-equation:

$$U_i \frac{\partial k}{\partial x_i} = \frac{\partial}{\partial x_i}\left(\frac{v_t}{\sigma_k}\frac{\partial k}{\partial x_i}\right) + P_k - \varepsilon. \tag{A.1}$$

ε-equation:

$$U_i \frac{\partial \varepsilon}{\partial x_i} = \frac{\partial}{\partial x_i}\left(\frac{v_t}{\sigma_\varepsilon}\frac{\partial \varepsilon}{\partial x_i}\right) + C_{1\varepsilon}\frac{\varepsilon}{k}P_k - C_{2\varepsilon}\frac{\varepsilon^2}{k}, \tag{A.2}$$

where

$$P_k = v_t\left(\frac{\partial U_i}{\partial x_j} + \frac{\partial U_j}{\partial x_i}\right)\frac{\partial U_i}{\partial x_j}, \tag{A.3}$$

$$v_t = C_\mu k^2/\varepsilon. \tag{A.4}$$

Wall function

$$U/u_* = \frac{1}{\kappa}\ln(E_{\text{wall}} y u_*/v), \tag{A.5}$$

where σ_k, σ_ε, $C_{1\varepsilon}$, $C_{2\varepsilon}$, and E_{wall}, are the model constants u_* is the wall friction velocity, v is the kinematic viscosity, and v_t is the turbulent eddy viscosity.